

See discussions, stats, and author profiles for this publication at: <https://www.researchgate.net/publication/272090125>

PbGa₂MSe₆ (M = Si, Ge): Two exceptional infrared nonlinear optical crystals

ARTICLE *in* CHEMISTRY OF MATERIALS · JANUARY 2015

Impact Factor: 8.35 · DOI: 10.1021/cm504195x

CITATIONS

3

READS

23

8 AUTHORS, INCLUDING:



Hao Zhang

Chinese Academy of Sciences

71 PUBLICATIONS 724 CITATIONS

[SEE PROFILE](#)



Hong Chen

KTH Royal Institute of Technology

44 PUBLICATIONS 114 CITATIONS

[SEE PROFILE](#)



Zhangzhen He

Chinese Academy of Sciences

127 PUBLICATIONS 940 CITATIONS

[SEE PROFILE](#)



Wen-Dan Cheng

Chinese Academy of Sciences

100 PUBLICATIONS 965 CITATIONS

[SEE PROFILE](#)

PbGa₂MSe₆ (M = Si, Ge): Two Exceptional Infrared Nonlinear Optical Crystals

Zhong-Zhen Luo,[†] Chen-Sheng Lin,[†] Hong-Hua Cui,[†] Wei-Long Zhang,[‡] Hao Zhang,[†] Hong Chen,^{§,||}
Zhang-Zhen He,[†] and Wen-Dan Cheng*,[†]

[†]State Key Laboratory of Structural Chemistry, Fujian Institute of Research on the Structure of Matter, Chinese Academy of Sciences, Fuzhou 350002, P. R. China

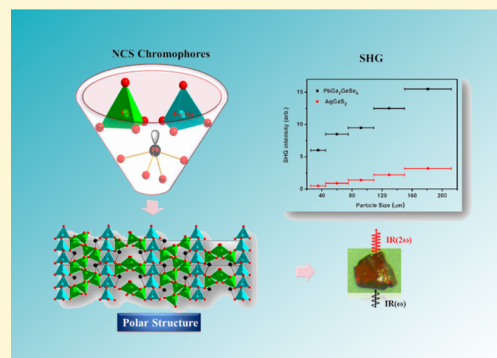
[‡]College of Electronics and Information Science, Fujian Jiangxia University, Fuzhou 350108, P. R. China

[§]Berzelii Center EXSELENT on Porous Materials and Department of Materials and Environmental Chemistry, Stockholm University, SE-106 91 Stockholm, Sweden

^{||}Faculty of Material Science and Chemistry, China University of Geosciences, Wuhan 430074, P. R. China

Supporting Information

ABSTRACT: Two noncentrosymmetric (NCS) quaternary selenides, PbGa₂SiSe₆ (**1**) and PbGa₂GeSe₆ (**2**), with second-order nonlinear optical (NLO) responses, were synthesized by a conventional high-temperature solid-state reaction method. Compounds **1** and **2** are constructed by three NCS chromophores, [PbSe₄], [GaSe₄], and [Ga/SiSe₄] or [Ga/GeSe₄], with the covalent interactions between the X and Se atoms (X = Pb, Ga, Ga/Si, or Ga/Ge). They crystallize in the polar space groups *Cc* and *Fdd2*, respectively. Inspiringly, compound **2** is phase-matchable (PM) and shows high laser-induced damage threshold (LIDT) of 3.7 × AgGaS₂ and wide transparent region (0.63–25 μm) in the mid-infrared (MIR) region. Most importantly, it presents extraordinary strong second harmonic generation (SHG) at 2.05 μm radiation of about 12 × AgGaS₂ at the particle size of 25–45 μm, which represents the strongest SHG among PM chalcogenides to date. The calculated major SHG tensor elements of compounds **1** and **2** are $d_{31} = 224.7$ and $d_{12} = 222.1$ pm/V, respectively, while the calculated d_{36} of AgGaS₂ is only 21.2 pm/V.



INTRODUCTION

Midinfrared (MIR) second-order nonlinear optical (NLO) materials have been widely applied in laser frequency conversion devices, which produce the coherent light source with important uses, such as molecular spectroscopy, atmospheric sensing, noninvasive medical diagnostics, laser guidance, deep-space detector, long-distance laser communication, various optoelectronic devices, etc.^{1–4} Compared with several outstanding NLO crystals, which have been widely used in the ultraviolet (UV) and visible regions, such as BaB₂O₄, LiB₃O₅, KTiOPO₄, LiNbO₃, and KBe₂BO₃F₂,^{1,5} there are only a few NLO crystals (e.g., chalcopyrite-type AgGaQ₂ (Q = S, Se) and ZnGeP₂) that are commercially available in the MIR region. However, these MIR NLO crystals have some drawbacks including low laser-induced damage thresholds (LIDTs), being nonphase-matchable at 1 μm, strong two-photon absorption, and difficulties in growing high-quality crystals.⁶ Because of these issues, the exploration for new high-quality MIR NLO crystals, which have (1) large NLO susceptibility (d_{ij}), (2) moderate birefringence (Δn) and phase-matchable (PM) property, (3) wide transparency region, (4) high LIDT, and (5) good chemical and thermal stability, is an urgent task in this field.

Recently, BaGa₄Q₇ (Q = S, Se) have been reported, which exhibit good NLO properties with large NLO coefficients, originating from the distorted tetrahedra [GaQ₄].^{7,8} And a series of compounds have been prepared in our lab by introducing the NLO active Sn²⁺ cation, such as Ba₇Sn₅S₁₅ and Ba₈Sn₄S₁₅, which exhibit excellent NLO properties about 2× and 10× AgGaS₂ at 2.05 μm radiation, respectively.^{9,10} These NLO responses are mainly originated from Sn(II)S₃ units for Ba₇Sn₅S₁₅ and Sn(II)₂S₃ units for Ba₈Sn₄S₁₅, which possess the stereochemically active lone pair (SCALP) electrons. In addition, Feng et al. reported that the compound Ba₆Sn₆Se₁₃ containing Sn(II)Se₃ trigonal pyramid and Sn(II)Se₅ quadrangular pyramid also shows moderate NLO response.¹¹ In order to improve the possibility of forming a noncentrosymmetric (NCS) crystal, two or more types of NCS chromophores, especially the NLO active units possessing SCALP electrons, are usually employed.^{12,13} On the basis of this idea, we have combined two NLO active NCS chromophores, distorted tetrahedra [GaQ₄] and Sn²⁺ cation,

Received: November 14, 2014

Revised: December 31, 2014

Published: January 6, 2015

for designing new NLO crystals. Two outstanding NLO compounds, SnGa_4Q_7 , have been synthesized in our lab.¹⁴ Remarkably, SnGa_4Se_7 is PM and exhibits large second harmonic generation (SHG) conversion efficiency of about $3.8 \times \text{AgGaS}_2$ at $2.05 \mu\text{m}$ radiation. The above-mentioned NCS compounds are shown in the quasi-ternary phase diagram of $\text{BaQ}-\text{Ga}_2\text{Q}_3-\text{Sn}(\text{Ss}^2)\text{Q}$ in Figure 1.

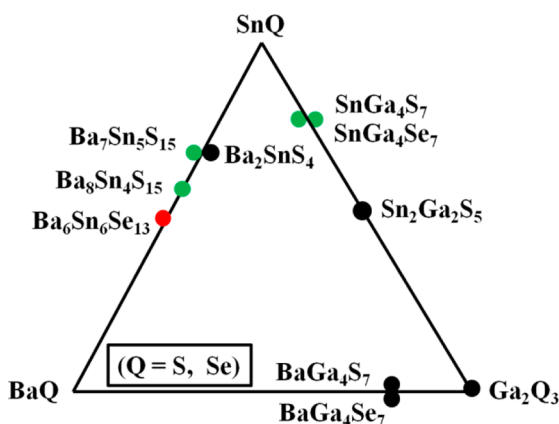


Figure 1. Primary NCS crystallization phases in the quasi-ternary phase diagram of $\text{BaQ}-\text{Ga}_2\text{Q}_3-\text{Sn}(\text{Ss}^2)\text{Q}$.

Inspired by these results, we tried to replace Sn^{2+} with Pb^{2+} so as to achieve the assumed product “ PbGa_4Se_7 ”. Single crystals of $\text{PbGa}_2\text{SiSe}_6$ (**1**) with space group Cc were obtained as a byproduct from experiments aiming at the single crystal growth of “ PbGa_4Se_7 ”. It was the first example ever reported in the $\text{Pb}-\text{Ga}-\text{Si}-\text{Se}$ system, and the Si in the compound originates from the silica tube. Then, another new NCS compound $\text{PbGa}_2\text{GeSe}_6$ (**2**) with space group $Fdd2$ has been obtained by replacing Si with Ge. Compounds **1** and **2** not only show interesting structural characteristics but also exhibit exceptional MIR NLO properties. Remarkably, compound **2** exhibits the strongest SHG response at $2.05 \mu\text{m}$ radiation that is about 12 times larger than that of benchmark AgGaS_2 at the particle size of $25-45 \mu\text{m}$ among the type-I PM chalcogenides. And the SHG conversion efficiency is about 5 times larger than that of AgGaS_2 at the particle size of $150-210 \mu\text{m}$.

■ EXPERIMENTAL SECTION

Reagents. The following chemicals in this work were used without further purification as obtained: Pb (Sinopharm Chemical Reagent Co., Ltd, 99.99%), Ga (Sinopharm Chemical Reagent Co., Ltd, 99.99%), Si (Sinopharm Chemical Reagent Co., Ltd, 99.99%), Ge (Sinopharm Chemical Reagent Co., Ltd, 99.99%), Se (Sinopharm Chemical Reagent Co., Ltd, 99.95%), and AgGaS_2 (bought from the company of CASTECH INC). PbSe and Ga_2Se_3 were prepared by stoichiometric reactions of the elements at 1073 and 1173 K, respectively, in the fused silica tubes evacuated to 10^{-2} Pa.

Synthesis. Crystals of $\text{PbGa}_2\text{SiSe}_6$ (**1**) were initially obtained from the reaction, which was to achieve the assumed product “ PbGa_4Se_7 ” with Pb, Ga, and Se in the molar ratio of 1:4:7. And then, the synthetic route has been optimized as follows: Compound **1** was synthesized from a mixture of PbSe (0.169 g, 0.593 mmol), Ga_2Se_3 (0.222 g, 0.593 mmol), Si (0.017 g, 0.593 mmol), and Se (0.093 g, 1.186 mmol). The reagents were mixed and ground carefully, homogenized thoroughly with ethanol (99.7%) in an agate mortar, and then pressed into sheets on the tablet machine. The prepared sheets were put in a predried silica tube and flame-sealed under a 10^{-2} Pa. Subsequently, the silica tube was placed in a muffle furnace and heated to 1023 K in 48 h, dwelled at that temperature for 50 h, and then was cooled at a rate of 3

K/h to 573 K followed by rapid cooling to room temperature. A few red crystals (about 10% yield based on Pb) of **1** were obtained with a large number of byproducts of PbGa_2Se_4 , SiSe_2 , and unreacted reagents. The crystals were air stable for at least five months and stable under ethanol and water.

$\text{PbGa}_2\text{GeSe}_6$ (**2**) was synthesized as follows: A mixture of PbSe (0.160 g, 0.565 mmol), Ga_2Se_3 (0.211 g, 0.565 mmol), Ge (0.041 g, 0.565 mmol), and Se (0.088 g, 1.130 mmol) was ground carefully, homogenized thoroughly with ethanol in an agate mortar, and pressed into sheets on the tablet machine. The prepared sheets were put in a predried silica tube and flame-sealed under a 10^{-2} Pa. Subsequently, the silica tube was placed in a muffle furnace and heated to 1073 K in 48 h, dwelled at that temperature for 50 h, and then was cooled at a rate of 3 K/h to 573 K followed by rapid cooling to room temperature. By comparison, a large number of bulk dark red crystals (about 90% yield based on Pb) of **2** were obtained with a small amount of PbGa_2Se_4 , GeSe_2 , and unreacted reagents. The crystals were air stable for at least five months and stable under ethanol and water.

Pure phases of **1** and **2** were produced by the stoichiometric mixtures of the $\text{Pb}/\text{Ga}/\text{Si}/\text{Se}$ and $\text{Pb}/\text{Ga}/\text{Ge}/\text{Se}$ molar ratio of 1:2:1:6. The mixtures were heated to 873 K in 24 h (dwelled at that temperature for 50 h) and then cooled down to room temperature in 24 h. In order to improve the homogeneity and purity, the resulting products were reground by using a mortar and pestle and heated again at the same temperature.

Elemental Analyses. Semiquantitative microprobe elemental analyses of the crystals were performed with a field emission scanning electron microscope (FESEM, JSM6700F) equipped with an energy dispersive X-ray spectroscope (EDX, Oxford INCA). Using this method, it confirmed the presence of the elements of Pb, Ga, Si, and Se for **1** and Pb, Ga, Ge, and Se for **2**. Moreover, the EDX analyses gave the empirical formulas of $\text{PbGa}_{2.1(2)}\text{Si}_{1.1(1)}\text{Se}_{6.0(9)}$ for **1** and $\text{PbGa}_{1.9(8)}\text{Ge}_{1.0(5)}\text{Se}_{5.9(8)}$ for **2**, which agree well with the single crystal refinement results (Supporting Information Figure S1).

Single-Crystal Structure Determination. Blocky single crystals of **1** and **2** were chosen for the single-crystal diffraction data collection. The data were collected with the use of graphite monochromated Mo K_α radiation ($\lambda = 0.71073 \text{ \AA}$) on a Saturn724+ and Saturn70 diffractometer at 293 K, respectively. Polarization effects, Lorentz, and semiempirical corrections were applied for data reduction. In addition, the absorption corrections were performed with the multiscan method.¹⁵ For the structure determination of **1**, the initial structure refinement generated one Pb, six Se, and three “Ga” atoms and an “unbalanced” formula of “ PbGa_3Se_6 ” with R values of $R_1 = 6.97\%$ and $wR_2 = 8.56\%$. The thermal parameters $U(\text{eq})$ are 0.014(3) for “Ga1”, 0.034(6) for “Ga2”, and 0.035(5) for “Ga3”, respectively. The EDX results suggested the existence of Si, and the molar ratio of Ga:Si is very close to 2:1. And the “Ga1”–Se distances [2.398(3)–2.454(4) \AA] are slightly longer than the “Ga2”–Se [2.283(4)–2.341(4) \AA] and “Ga3”–Se [2.302(4)–2.329(4) \AA]. Subsequently, two of the “Ga”, which had big thermal parameter, and Si were constrained to share the same crystallographic sites and freely refined. Because the site occupation factors of Si(2)/Ga(2) and Si(3)/Ga(3) were very close to these values of 0.5 and 0.5, the values were subsequently fixed. This treatment yielded a much smoother residual electron density and a neutral formula of “ $\text{PbGa}_2\text{SiSe}_6$ ”, which agreed well with the EDX results and much better R values of $R_1 = 3.63\%$, $wR_2 = 7.69\%$ with the thermal parameters of the three “Ga”, 0.015(1) for Ga(1), 0.012(1) for Ga(2)Si(2), and 0.013(1) for Ga(3)Si(3), respectively.

While for **2**, though the Ga and Ge atoms are virtually indistinguishable by single-crystal X-ray diffraction, by combination with the EDX results, thermal parameters, bond lengths, and charge balance, the structure refinement was treated by the similar procedure as that for **1**. Two structures were solved by direct method and refined on F^2 by a full-matrix least-squares method using the SHELXL-97 programs.¹⁶ All of the atoms were refined with anisotropic thermal parameters. The final refined crystal structures of **1** and **2** were checked by using the program PLATON,¹⁷ and there were no missed or higher symmetry elements to be found. The crystallographic details for **1** and **2** are listed in Table 1. The atomic coordinates, equivalent

isotropic thermal parameters, and important bond distances and bond angles are given in Tables S1 and S2 (see the Supporting Information).

Table 1. Crystal Data and Structural Refinement Details for 1 and 2

chemical formula	PbGa ₂ SiSe ₆ (1)	PbGa ₂ GeSe ₆ (2)
formula weight	848.49	893.01
space group	<i>Cc</i>	<i>Fdd2</i>
<i>a</i> (Å)	7.188(5)	47.135(16)
<i>b</i> (Å)	23.171(19)	7.578(3)
<i>c</i> (Å)	7.044(5)	12.161(4)
β (deg)	116.25(3)	90
<i>V</i> (Å ³), <i>Z</i>	1052.2(14), 4	4344(3), 16
ρ_{cal} (g cm ⁻³)	5.356	5.462
absorption correction	multiscan	multiscan
absorption coefficient (mm ⁻¹)	41.844	43.145
crystal size (mm)	0.15 × 0.10 × 0.08	0.20 × 0.10 × 0.06
<i>F</i> (000)	1448	6080
R_1^a , wR_2^b , for $I > 2\sigma(I)$	0.0368, 0.0774	0.0269, 0.0492
R_1^a , wR_2^b , for all data	0.0503, 0.1209	0.0315, 0.0506
GOF on <i>F</i> ²	0.962	0.946
$^a R_1 = \sum F_o - F_c / \sum F_o . \quad ^b wR_2(F_o^2) = [\sum w(F_o^2 - F_c^2)^2 / \sum w(F_o^2)^2]^{1/2}.$		

Powder X-ray Diffraction. The powder X-ray diffraction (PXRD) patterns were recorded on a Rigaku MiniFlex II diffractometer with Cu K α radiation in reflection mode at room temperature with a step size of 0.02° and a scan speed of 0.15°/min. Both the experimental and simulated PXRD patterns of **1** and **2** are shown in Figure S2 in the Supporting Information. In addition, Le Bail fitting was carried out in Jana 2006¹⁸ for both PXRD patterns as shown in Supporting Information Figure S3. On the basis of the crystallographic information obtained from single-crystal X-ray diffraction, the Le Bail fitting of the profiles converged to the final R_p , R_{wp} , and GOF values of 8.85%, 11.49%, and 1.51 for **1** and 4.92%, 6.96%, and 1.44 for **2**, respectively. No impurity peaks were observed in the difference profile, which indicated a high purity of the as-synthesized samples.

Solid-State UV–Vis and IR Spectroscopy. The UV–vis diffuse reflectance spectra were recorded at room temperature on a PerkinElmer Lambda 900 UV–vis spectrometer in the range of 200–2500 nm with BaSO₄ as a reference. The absorption spectra were calculated from the diffuse reflectance spectra using the Kubelka–Munk function: $\alpha/S = (1-R)^2/2R$, where α is the absorption coefficient, S is the scattering coefficient, and R is the reflectance.¹⁹

The IR spectra were recorded on a PerkinElmer Spectrum One FR-IR Spectrometer in the range of 2.5–25 μm (400–4000 cm⁻¹) at room temperature. The samples were diluted with dry KBr and pressed into transparent sheets on the tablet machine.

SHG Measurements. The SHG responses test of **2** was performed on crystalline samples by using the Kurtz and Perry method with 2.05 μm Q-switch laser.²⁰ The samples were measured in particle size ranges of 25–45, 45–74, 74–106, 106–150, and 150–210 μm and pressed into disks with diameter of 8 mm. AgGaS₂ crystal was ground and sieved into the same size range as the reference. The SHG conversion efficiency is defined as $\eta = I_{2\omega}/I_{\omega}$ which is a rate of SHG and incident light intensities. Accordingly, the relative SHG conversion efficiency can be derived based on the measurements of size-dependent powder SHG intensities of sample and reference.

Powder LIDTs Measurements. The single pulse measurement method was used to estimate the powder LIDT of compound **2** with AgGaS₂ as the reference.²¹ The same particle size samples (25–45 μm) of **2** and AgGaS₂ were selected and pressed into disks with diameter of 8 mm. The color changes of the samples were observed by the optical microscope when high-power 1064 nm laser radiation passed with a pulse width τ_p of 8 ns. Meanwhile, the Nova II sensor with a PESO-DIF-C energy sensor and vernier caliper were respectively

used to measure the power of laser beam and damage spots, which showed the color changes.

Thermal Analyses. Thermogravimetric analysis (TGA) of compounds **1** and **2** were performed on a NETZSCH STA 449C thermal under N₂ flow at a rate of 30 mL/min and a Mettler Toledo TGA/SDTA 851e under air, respectively. About 8 mg of powder samples were placed in Al₂O₃ crucibles and heated from 30 to 800 °C at 10 °C/min.

Electronic Structure Calculations. Energy band structure and optical properties of **1** and **2** were completed by using density functional theory (DFT) calculation with CASTEP code²² provided by Material Studio (MS) package. Interaction of the electrons with ion cores was represented by the norm-conserving pseudopotentials for **1** and **2**. The valence electrons were treated as Pb: 6s²6p², Ga: 3d¹⁰4s²4p¹, Si: 3s²3p² (Ge: 4s²4p² for **2**), and Se: 4s²4p⁴. The exchange and correlative potentials of electron–electron interactions were described by using the generalized gradient approximation (GGA) in the scheme of Perdew–Burke–Erzerhof (PBE).²³ The *k*-point of first Brillouin zone (BZ) for both compounds was sampled as 2 × 2 × 2 Monkhorst–Pack scheme.²⁴ Energy cutoff and precision for both compounds were set to be 700 eV and 2.0 × 10⁻⁶ eV/atom, respectively. The dipole moments (μ) of the [PbSe₄]_n, [GaSe₄]_n, [SiSe₄]_n, and [GeSe₄]_n units were calculated from the charge distribution of Bader analysis based on the DFT cacuation implemented in VASP package.²⁵ The X-ray crystal structure data were used without further optimization on the basis of two ordered structures. For compound **1**, the (Ga(2)/Si(2)) and (Ga(3)/Si(3)) positions were set as Si and Ga atoms, respectively. For compound **2**, the (Ga(3)/Ge(3)) and (Ga(4)/Ge(4)) positions were set as Ge and Ga atoms, respectively.

The theoretical studies of optical properties for the title compounds in terms of the complex dielectric function $\epsilon(\omega) = \epsilon_1(\omega) + i\epsilon_2(\omega)$ are given by

$$\epsilon_2^{ij}(\omega) = \frac{8\pi^2\hbar^2e^2}{m^2V_{\text{eff}}} \sum_k \sum_{cv} (f_c - f_v) \frac{p_{cv}^i(k)p_{vc}^j(k)}{E_{vc}^2} \delta[E_{cv}(k) - \hbar\omega] \quad (1)$$

where $\delta[E_{cv}(k) - \hbar\omega] = \delta[E_c(k) - E_v(k) - \hbar\omega]$ indicates the energy difference between the conduction bands (CB) and valence bands (VB) at the *k* point with absorption of a quantum $\hbar\omega$. The f_c and f_v represent the Fermi distribution functions of the CB and VB, respectively. The term $p_{cv}^i(k)$ denotes the momentum matrix element transition from the energy level *c* of the CB to the level *v* of the VB at the *k* point in the BZ and *V* is the volume of the unit cell. The *m*, *e*, and \hbar are the electron mass, charge, and Planck's constant, respectively. Then the first-order susceptibility at low frequency region is given by $\chi^{(1)}(\omega)_{ii} = [\epsilon(\omega)_i - 1]/4\pi$. The second-order susceptibilities can be expressed in terms of the first-order susceptibilities as follows:

$$\chi_{ijk}^{(2)}(-\omega_3; \omega_1, \omega_2) = F^{(2)} \chi_{ii}^{(1)}(\omega_3) \chi_{jj}^{(1)}(\omega_1) \chi_{kk}^{(1)}(\omega_2) \quad (2)$$

where $F^{(2)} = ma/(N^2e^3)$. All of the expressions are derived from a classical anharmonic oscillator (AHO) model.²⁶ The *m* and *e* are the electron mass and charge, respectively. The parameter *a*, which characterizes the nonlinearity of the response, is estimated by ω_0^2/l , where *l* and ω_0 are the lattice constant and response frequency, respectively. *N* is the density number of unit cell. For compounds **1** and **2**, *F* is estimated to be 4.73×10^{-6} and 5.04×10^{-6} esu, respectively. The SHG components d_{ij} is equal to half of the corresponding χ_{ij} value for the consequence of historical convention.

■ RESULTS AND DISCUSSION

Crystal Growth. Several crystal growth attempts, including a muffle furnace and a two-zone vertical furnace, were conducted to get the large-sized crystal of **1** for the measurement of NLO properties. Unfortunately, the single crystals of **1** are too small and few to be measured. Contrarily,

the crystal growth of **2** is very easy and the crystal is of high-quality (Supporting Information Figure S6).

Crystal Structure. *Structure of PbGa₂SiSe₆, 1.* Compound **1** crystallizes in the polar space group *Cc* of the monoclinic system with $a = 7.188(5)$ Å, $b = 23.171(19)$ Å, $c = 7.044(5)$ Å, $\beta = 116.25(3)^\circ$, and $Z = 4$. In the asymmetric unit, there is crystallographically one Pb atom, one Ga atom, two metal positions randomly occupied by both Ga and Si in the molar ratio of 1:1, and six Se atoms. The Pb atom is coordinated by four Se atoms to form [PbSe₄] tetra-pyramid (Figure 2a) with

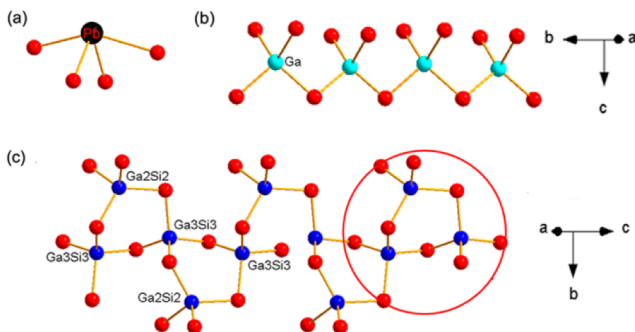


Figure 2. [PbSe₄] tetra-pyramid (a), the structure of infinite 1^{∞} [GaSe₄] chain (b), and the infinite 1^{∞} [(Ga/Si)₃Se₉] zigzag chain formed by the trioxane-like SSU [(Ga/Si)₃Se₉] unit (in the red circle) (c) of **1**. (Black, Pb; turquoise, Ga; blue, (Ga/Si); red, Se.)

the Pb–Se distances ranging from 2.915(3) to 3.233(3) Å, which are comparable to those of 2.707 to 3.321 Å in Fe_{0.96}Pb_{3.04}Sb₄Se₁₀.²⁷ Both the Ga atom and (Ga/Si) positions are coordinated to four Se atoms forming tetrahedra, with the Ga–Se and (Ga/Si)–Se distances ranging from 2.398(3) to 2.454(4) and 2.284(3) to 2.340(3) Å, respectively. The distances of Ga–Se and (Ga/Si)–Se are close to those of 2.422 Å in GaTa₄Se₈^{28,29} and 2.347(2) to 2.372(2) Å in BaGa₂SiSe₆.³⁰ The [GaSe₄] tetrahedra stack on top of each other by sharing the corners and string to make an infinite 1^{∞} [GaSe₄] chain (Figure 2b). Interestingly, the three [(Ga/Si)Se₄] tetrahedra form the trioxane-like secondary structure unit (SSU), [(Ga/Si)₃Se₉], as shown in Figure 2c. These SSUs connect to each other by sharing the [(Ga/Si)Se₄] tetrahedra and form the infinite 1^{∞} [(Ga/Si)₃Se₉] zigzag chain (Figure 2b). Finally, the infinite 1^{∞} [GaSe₄] and 1^{∞} [(Ga/Si)₃Se₉] zigzag chains construct the 3D framework by alternated stacking along the *b*-axis and *c*-axis, respectively (Figure 3). The [PbSe₄] tetra-pyramids are located in the cavities formed by the infinite 1^{∞} [GaSe₄] and 1^{∞} [(Ga/Si)₃Se₉] zigzag chains.

Structure of PbGa₂GeSe₆, 2. Compound **2** crystallizes in the polar space group *Fdd2* of the orthorhombic system with $a = 47.147(5)$ Å, $b = 7.5775(6)$ Å, $c = 12.1648(9)$ Å, and $Z = 16$. In the asymmetric unit, there are one crystallographically Pb atom, two Ga atoms, two independent metal positions randomly occupied by both Ga and Ge in the molar ratio of 1:1, and six Se atoms. The Pb atom is coordinated by four Se atoms to form tetra-pyramid with the Pb–Se distances ranging from 2.9114(12) to 3.2690(15) Å. These Pb–Se distances are comparable to those of 2.707 to 3.321 Å in Fe_{0.96}Pb_{3.04}Sb₄Se₁₀.²⁷ All of the Ga atoms and (Ga/Ge) positions are bonded to four Se atoms forming the [GaSe₄] and [(Ga/Ge)Se₄] tetrahedra, respectively, with the Ga–Se distances ranging from 2.4150(15) to 2.4380(15) Å and (Ga/Ge)–Se distances ranging from 2.3532(15) to 2.3788(14) Å.

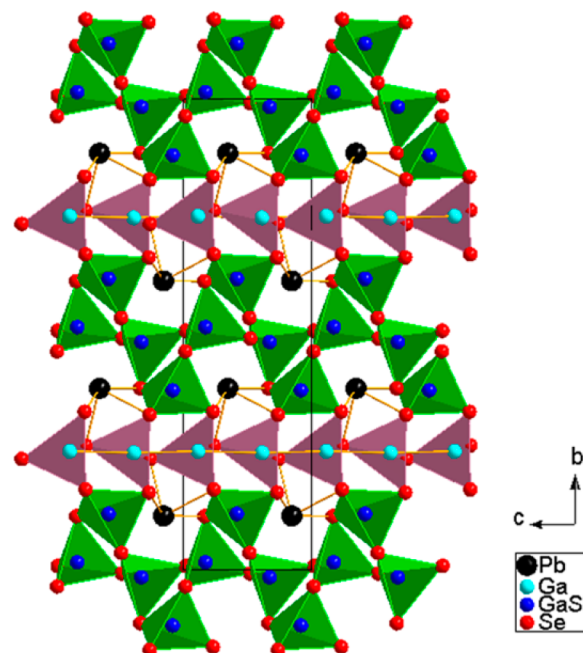


Figure 3. Tetrahedron packing of **1** viewed down the *a*-axis with the unit cell marked. Color code: black, Pb; turquoise, Ga; blue, (Ga/Si); red, Se; bright green, (Ga/Si)Se₄ tetrahedron; rose, Ga₃Si₃ tetrahedron.

These Ga–Se and (Ga/Ge)–Se distances are close to those of 2.422 Å in GaTa₄Se₈^{28,29} and those in CuGaGeSe₄ (2.374 Å).³¹ Similar to compound **1**, the [GaSe₄] tetrahedra also form the infinite 1^{∞} [GaSe₄] chain. And the trioxane-like SSUs, [(Ga/Ge)₃Se₉], construct the infinite 1^{∞} [(Ga/Ge)₃Se₉] zigzag chain. Then the infinite 1^{∞} [GaSe₄] and 1^{∞} [(Ga/Ge)₃Se₉] zigzag chains form the 3D framework, by alternated stacking along the *b*-axis and *c*-axis, respectively (Figure 4). And, the [PbSe₄] tetra-pyramids are located in the cavities formed by the infinite 1^{∞} [GaSe₄] and 1^{∞} [(Ga/Ge)₃Se₉] zigzag chains as well as **1**.

Interestingly, although Pb, Ga, Se, and Si/Ge atoms have the same coordination types in the two compounds, compounds **1** and **2** have different space groups due to the slightly different radii of Si and Ge. Some other examples, such as Ba₂BiInS₅ (*Cmc*₂₁) and Ba₂BiGaS₅ (*Pnma*),³² Ba₂In₂S₅ (*Pbca*)³³ and Ba₂Ga₂S₅ (*C2/c*),³⁴ Ba₄In₂S₈ (*P1*) and Ba₄Ga₂S₈ (*P2*₁/*c*),³⁵ and Ln₄GaSbS₉ (Ln = Pr, Nd, Sm, Gd–Ho) (*Aba*₂)³⁶ and Ln₄InSbS₉ (Ln = La, Pr, Nd) (*P4*₁2₁2),³⁷ show that slight radius change would result in different structure packing patterns of the similar asymmetric units. Moreover, due to the fact that slight changes of elements would result in a huge variety of crystal structures, those systems provide an enormous playground for a further fundamental understanding of composition–structure–property relationships.

Optical Properties. The band gaps of the title compounds were determined with diffuse-reflectance UV–vis/near-IR spectra. The experimental results give the band gaps of 2.17 and 1.96 eV for **1** and **2**, respectively, which are consistent with the red colors (Figure 5). Both the band gaps of **1** and **2** are larger than that of AgGaSe₂ (1.8 eV). A high LIDT in a NLO crystal usually corresponds to a large energy band gap, which is very helpful to improve the LIDTs of compounds.³⁸ As shown in Figure 5, there are no obvious optical absorption peaks in the IR transmission spectra of **1** and **2**. Thus, both of them have wide transparent regions from 0.57 to 25 and 0.63 to 25 μm,

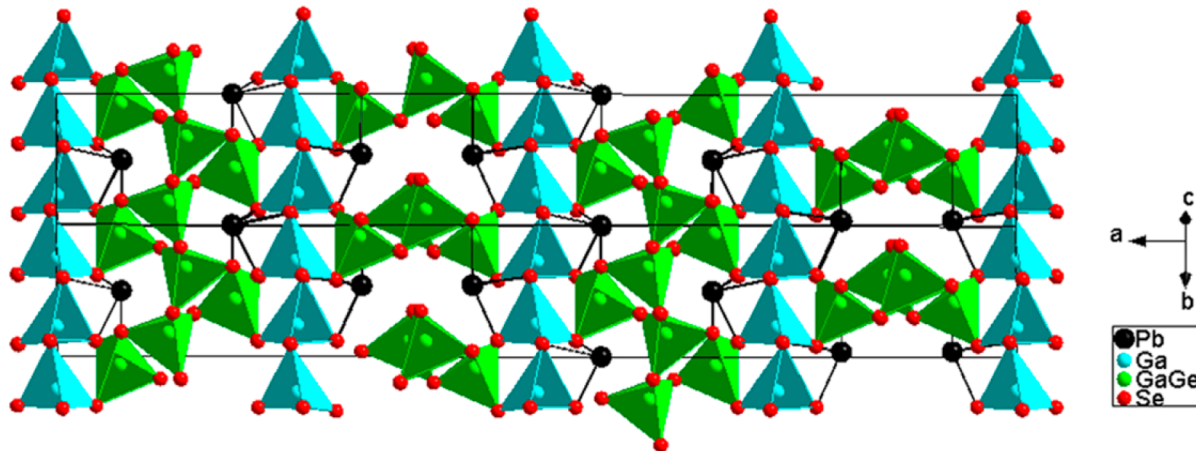


Figure 4. Approximate (113) structure view of 2. (Black, Pb; turquoise, Ga; green, (Ga/Ge); red, Se; turquoise tetrahedron, GaSe_4 ; green tetrahedron, $(\text{Ga/Ge})\text{Se}_4$.)

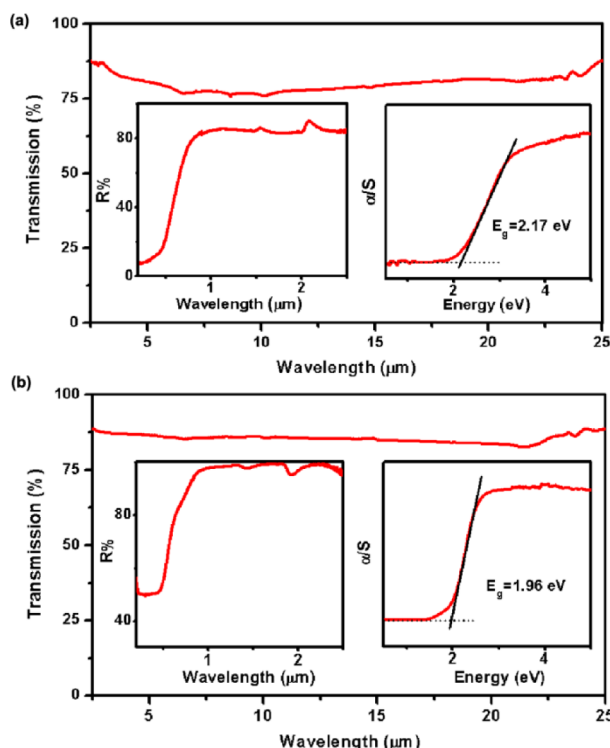


Figure 5. Reflection spectra, UV-vis diffuse reflectance spectra (inset panel), and IR spectra of 1 (a) and 2 (b).

respectively, which cover the two important atmospheric transparent windows (3–5 and 8–14 μm).³⁹

NLO Properties. Because of the polar space group $Fdd2$ and broad transparency in the MIR region, the SHG of 2 has been investigated with a 2.05 μm Q-switch laser and AgGaS₂ as a reference. The particle size versus the SHG response curve is shown in Figure 6a. The SHG intensities of 2 increased with the increasing particle size, which indicates a type-I PM nature. It is highly favorable for NLO performance. Remarkably, the SHG intensities of 2 are about 12 and 5 times those of commercial AgGaS₂ at the particle size of 25–45 and 150–210 μm (Figure 6b), respectively. Accordingly, the ratio of $\eta^2/\eta^{\text{AgGaS}_2} = I^2(2\omega)/I^{\text{AgGaS}_2}(2\omega)$ is calculated to be approximately 5.0 at the same input intensity $I(\omega)$ and particle size of 150–210 μm. This value indicates that the nonlinear conversion

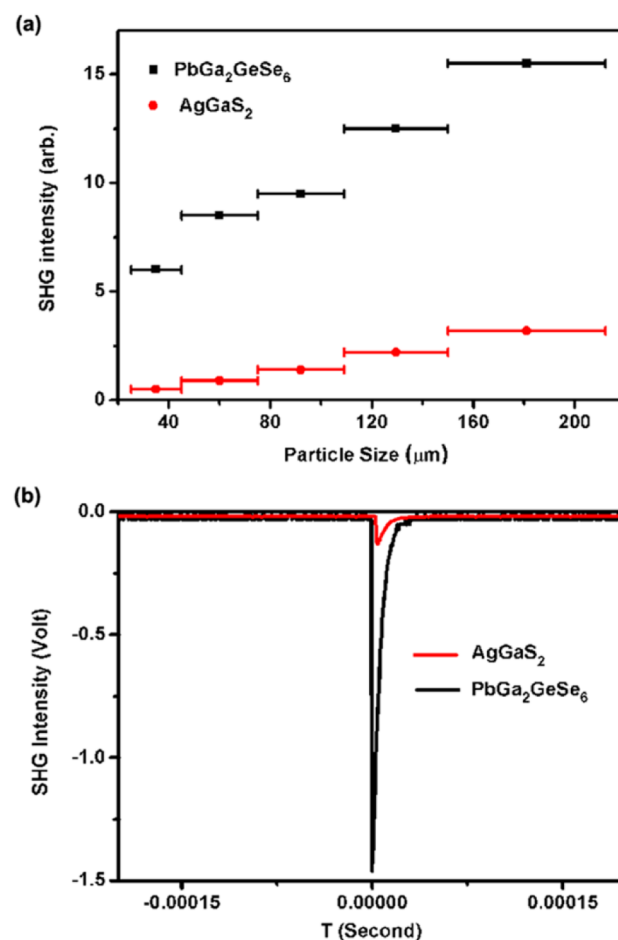


Figure 6. SHG intensities of 2 with AgGaS_2 as a reference: (a) PM curves, i.e., particle size versus SHG response; (b) oscilloscope traces of SHG signals at a particle size of 25–45 μm.

efficiency of sample 2 is about 5.0 times as compared with that of reference AgGaS_2 . Besides, the SHG response was detected when the powder of compound 1 was investigated with a 2.05 μm Q-switch laser.

Powder LIDTs. The experimental results of powder LIDTs for 2 and AgGaS_2 (as a reference) are summarized in Table 2. With the same spot diameter of 6.50 mm, the damage energy of

Table 2. Laser LIDTs of $\text{PbGa}_2\text{GeSe}_6$ and AgGaS_2 (as the reference)

compounds	damage energy (mJ)	spot diameter (mm)	damage threshold (MW/cm^2)
$\text{PbGa}_2\text{GeSe}_6$	14.90	6.50	5.61
AgGaS_2	4.06	6.50	1.53

2 (14.90 mJ) is much larger than that of AgGaS_2 (4.06 mJ). And the LIDT of **2** ($5.61 \text{ MW}/\text{cm}^2$) is about 3.7 times as much as commercial AgGaS_2 ($1.53 \text{ MW}/\text{cm}^2$). All the above results imply that compound **2** is of enormous potential in high power ($P_{\text{avg}} > 1 \text{ kW}$) frequency conversion in the MIR region.⁴⁰

Thermal Stabilities. The TGA measurement results of **1** and **2** in N_2 and air are shown in Figure S4 (Supporting Information). As can be seen, the thermal stabilities of the compounds **1** and **2** can be up to 350 and 600 °C in N_2 and up to 330 and 520 °C in air (Supporting Information Figure S4c,d). Although the thermal stabilities of **1** and **2** in air are lower than in N_2 , which may be caused by the oxidation, these results indicate that **1** and **2** have good thermal stabilities. In addition, the main TGA residues of **1** and **2** are analyzed by the powder X-ray diffraction patterns (Supporting Information Figure S5). As shown in Supporting Information Figure S5, the TGA residues are PbGa_2Se_4 , Si, and PbSe for **1** and PbGa_2Se_4 , Si, and PbSe for **2** in N_2 . While in air, the main TGA residues are PbSe, PbO, Pb_3SiO_5 , Ga_2O_3 , and SiSe_2 for **1** and PbSe, $\text{Pb}_3\text{Ga}_2\text{Ge}_4\text{O}_{11}$, PbO, and Ga_2O_3 for **2**.

Electronic Structures. The electronic band structure and density of states (DOS) of **1** and **2** were calculated by the DFT to investigate the nature of the band gaps. As shown in Figure 7, the electronic band structures of the first BZ show that both **1** and **2** have indirect band gaps. For **1**, the highest occupied VB and the lowest unoccupied CB are located at the G point and the GZ line near the Z point with the band gap of 1.85 eV. As for **2**, the VB and CB are occupied by the G point and near the middle point between G and Z points with the band gap of 1.46 eV. Compared with the experimental results (2.17 eV for **1** and 1.96 eV for **2**), the calculated band gaps of **1** and **2** are underestimated. This is a well-known problem of semilocal functional approximation like GGA.^{41,42}

Although compounds **1** and **2** crystallize in different space groups, they have the similar DOS with the same coordinations of Pb, Ga, Se, and Si/Ge atoms in the two compounds. Thus, the partial density of states (PDOS) of **1** will be discussed as a representative. As shown in Figure 8a, the top of the VB (near the Fermi level) primarily contains Se-4p, Ga-4p, Si-3p, and Pb-6p states mixing with a small part of Se-4s and Pb-6s states, while the bottom of the CB is composed of Se-4s/-4p, Ga-4s/-4p, Si-3s/-3p, and Pb-6p states with a little mixture of the Pb-6s state. To sum up, the optical absorption of **1** originates from the electronic transitions from the Ga-Se, Si-Se, and Pb-Se bonding states to their antibonding states. Similarly, the optical absorption of **2** results from the Ga-Se, Ge-Se, and Pb-Se bonding states to their antibonding states as shown in Figure 8b.

Micromechanism of the NLO Responses. In order to obtain a deeper understanding of NLO responses of **1** and **2**, the dipole moments (μ) of the $[\text{PbSe}_4]$, $[\text{GaSe}_4]$, $[\text{SiSe}_4]$, and $[\text{GeSe}_4]$ units were calculated from the charge distribution of Bader analysis based on the DFT calculation implemented in the VASP package. The dipole moments are listed in Table 3 and marked by arrowheads in Figures 9 and 10. These results

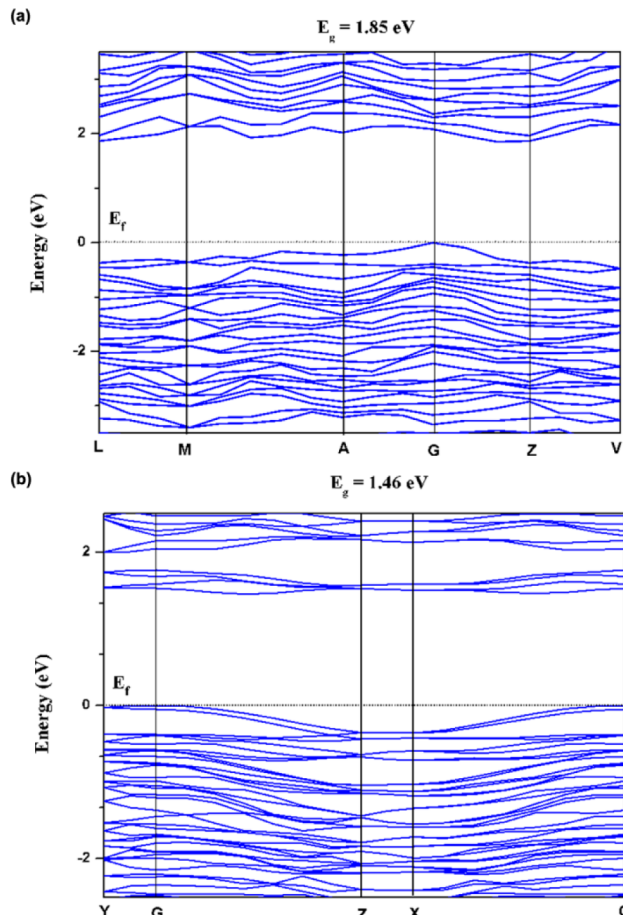


Figure 7. Electronic band structures of **1** (a) and **2** (b).

imply that the polarization of the $[\text{PbSe}_4]$ unit is much larger than those of the distorted tetrahedral $[\text{GaSe}_4]$, $[\text{SiSe}_4]$, and $[\text{GeSe}_4]$ units. It is found from Figures 9 and 10 that the local dipole moments of the $[\text{PbSe}_4]$ are enhanced along the z direction (Figure 9) and y direction (Figure 10) in the unit cell. And these enhancement effects result in large SHG responses of the two compounds. The obvious difference between the dipole moments of $[\text{PbSe}_4]$ units and distorted tetrahedra results from the lone pair electrons of stereochemical activity in the $[\text{PbSe}_4]$ unit. The partial electron density (PED) of compound **2** is shown in Figure 11, in which the SCALP electrons of Pb^{2+} are visualized. An almost spherical electron distribution can be seen around the Se atoms, while an asymmetric density distribution is clearly present around each Pb atom directed away from their nearest-neighboring Se atom (s-state is spherical electron distribution). Additionally, the weak covalent interactions between the Pb and Se atoms in compound **2** can be also observed from Figure 11. Thus, the $[\text{PbSe}_4]$ unit can make more contributions to the NLO responses of **1** and **2** than the distorted tetrahedral $[\text{GaSe}_4]$, $[\text{SiSe}_4]$, and $[\text{GeSe}_4]$ units.

As the space group of compound **1** belongs to class m , there are 10 nonvanishing tensors ($d_{11}, d_{12}, d_{13}, d_{15}, d_{24}, d_{26}, d_{31}, d_{32}, d_{33}$, and d_{35}). Only six independent tensors ($d_{11}, d_{12}, d_{13}, d_{15}, d_{24}$, and d_{33}) are taken into consideration judged by the Kleinman's symmetry. Those tensor components have very large values of 197.7, 222.1, 193.6, 195.6, 209.1, and 191.6 pm/V for $d_{11}, d_{12}, d_{13}, d_{15}, d_{24}$, and d_{33} , respectively, at a wavelength of 2.05 μm (0.60 eV). But for compound **2**, there are five

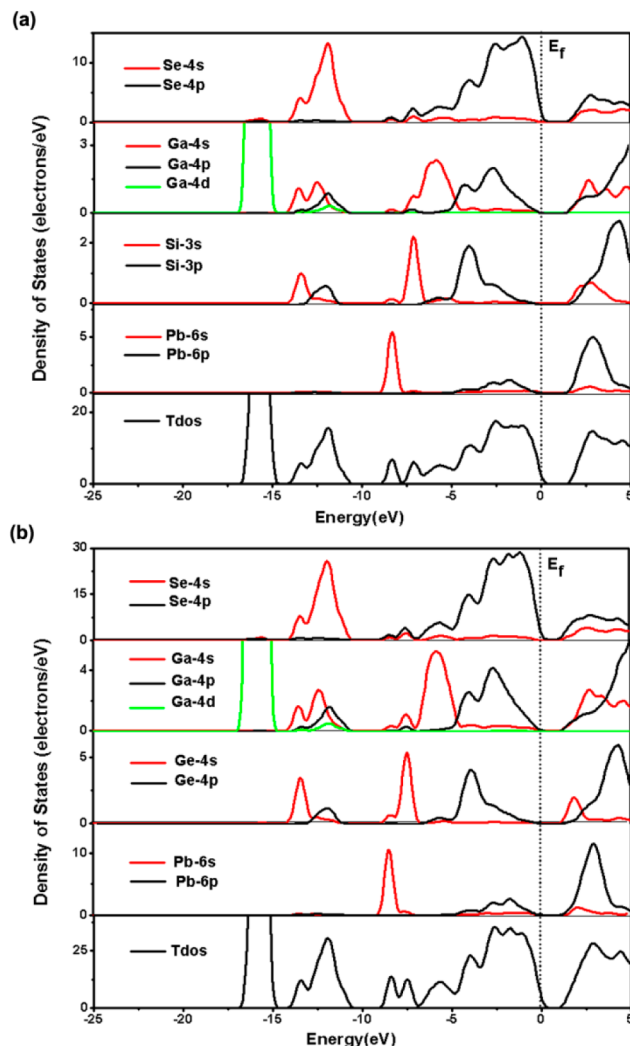
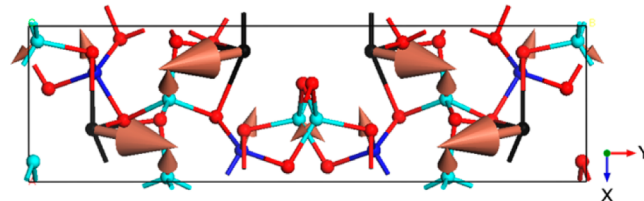


Figure 8. TDOS and PDOS of 1 (a) and 2 (b).

Table 3. Calculative Dipole Moment (Debye) μ of $[\text{PbSe}_4]$, $[\text{GaSe}_4]$, and $[\text{SiSe}_4]$ Units for 1 and $[\text{PbSe}_4]$, $[\text{GaSe}_4]$, and $[\text{GeSe}_4]$ Units for 2

unit	<i>x</i>	<i>y</i>	<i>z</i>	total dipole moment
$\text{PbGa}_2\text{SiSe}_6$ (1)				
$[\text{PbSe}_4]$	3.777	17.859	11.241	21.437
$[\text{Ga(1)}\text{Se}_4]$	-1.268	0.044	1.679	2.104
$[\text{Ga(3)}\text{Se}_4]$	0.943	-1.096	-0.163	1.456
$[\text{Si(2)}\text{Se}_4]$	-1.849	-0.614	0.663	2.058
$\text{PbGa}_2\text{GeSe}_6$ (2)				
$[\text{PbSe}_4]$	16.972	6.927	-4.545	18.887
$[\text{Ga(1)}\text{Se}_4]$	-0.469	-2.191	1.635	2.774
$[\text{Ga(2)}\text{Se}_4]$	0.0	0.0	0.926	0.926
$[\text{Ga(4)}\text{Se}_4]$	0.0	0.0	0.283	0.283
$[\text{Ge(3)}\text{Se}_4]$	0.846	-1.052	-1.175	1.790

nonvanishing tensors (d_{15} , d_{24} , d_{31} , d_{32} , and d_{33}) of second-order susceptibility due to the space group belonging to class *mm2*. And judging from the Kleinman's symmetry, only three independent tensors (d_{31} , d_{32} , and d_{33}) are taken into account. Those tensor components also have very large values, which are 187.3, 204.3, and 224.7 pm/V for d_{31} , d_{32} , and d_{33} , respectively, at a wavelength of 2.05 μm (0.60 eV). The computational

Figure 9. Dipole moments of the $[\text{PbSe}_4]$, $[\text{GaSe}_4]$, and $[\text{SiSe}_4]$ units of 1 shown by different arrowheads. For a clear illustration, arrowheads representing the dipole moments of $[\text{PbSe}_4]$ are reduced five times. (Turquoise, Ga; blue, Si; red, Se; black, Pb.)

results of 1 and 2 are shown in Figure 12 with d_{36} of AgGaS_2 as a reference.

Additionally, with the energy from 0 to 2 eV, the calculated refractive index (n) values of 1 and 2 range from 2.824 to 3.418 and 2.780 to 3.444, respectively (Figure S7, Supporting Information). As shown in Supporting Information Figure S8, the static Δn are 0.087 and 0.114 for 1 and 2 at a wavelength of 2.05 μm (0.60 eV), respectively, which are significantly larger than that of AgGaS_2 (0.039).⁴³ The moderate Δn of compound 1 is more than twice the value of AgGaS_2 at the wavelength of 2.05 μm , which indicates that compound 1 may achieve the PM conditions for SHG production in the MIR region.⁴⁴

CONCLUSIONS

In conclusion, a new family of NCS quaternary selenides, $\text{PbGa}_2\text{SiSe}_6$ (1) and $\text{PbGa}_2\text{GeSe}_6$ (2), have been synthesized and characterized. Compounds 1 and 2 crystallize in the polar space groups *Cc* and *Fdd2*, respectively. The 3D frameworks of the two compounds are composed of infinite ${}_1^{\infty}[\text{GaSe}_4]$ chains and ${}_1^{\infty}[(\text{Ga/Si})_3\text{Se}_9]$ zigzag chains for 1 (${}_1^{\infty}[(\text{Ga/Ge})_3\text{Se}_9]$ zigzag chains for 2) with $[\text{PbSe}_4]$ tetra-pyramids in the cavities, in which Pb is coordinated by four Se atoms via weak covalent interactions. Interestingly, the infinite ${}_1^{\infty}[(\text{Ga/Si})_3\text{Se}_9]$ and ${}_1^{\infty}[(\text{Ga/Ge})_3\text{Se}_9]$ zigzag chains are formed by the trioxane-like SSUs, $[(\text{Ga/Si})_3\text{Se}_9]$ and $[(\text{Ga/Ge})_3\text{Se}_9]$, respectively. The two compounds, containing three types of NCS chromophores ($[\text{PbSe}_4]$, $[\text{GaSe}_4]$, and $[\text{Ga/SiSe}_4]$ in 1 and $[\text{PbSe}_4]$, $[\text{GaSe}_4]$, and $[\text{Ga/GeSe}_4]$ in 2), can exhibit significant SHG responses and good optical performances in the MIR range. Remarkably, compound 2 shows a strong SHG at 2.05 μm radiation of about 12 times that of the benchmark AgGaS_2 at the particle size of 25–45 μm and a large SHG conversion efficiency at the particle size of 150–210 μm (5 times of AgGaS_2). It is the strongest SHG among type-I PM chalcogenides to date. These experimental results agree well with the calculated major SHG tensor elements, $d_{12} = 222.1 \text{ pm/V}$ for 1 and $d_{31} = 224.7 \text{ pm/V}$ for 2 (the calculated d_{36} of commercial AgGaS_2 is only 21.2 pm/V). In addition, the theoretical results indicate that the SCALP electrons of Pb^{2+} can significantly improve the polarity of the $[\text{PbSe}_4]$ unit and the polarization of the $[\text{PbSe}_4]$ unit is much larger than those of the distortion tetrahedral $[\text{GaSe}_4]$ and $[\text{SiSe}_4]$ units for 1 ($[\text{GaSe}_4]$ and $[\text{GeSe}_4]$ for 2). And the enhancements of the dipole moments of $[\text{PbSe}_4]$ groups along the certain directions in a cell can make significant contributions to NLO responses of the title compounds. Because of the exceptional performance with large SHG conversion efficiencies, type-I PM, high LIDT, good thermal stability, and wide MIR transparent regions extending to more than 25 μm , compound 2 is expected to be a new promising candidate for NLO crystals in the MIR region. The research

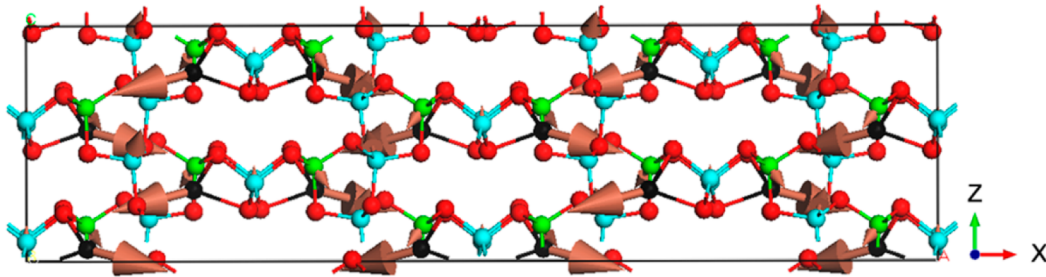


Figure 10. Dipole moments of the $[\text{PbSe}_4]$, $[\text{GaSe}_4]$, and $[\text{GeSe}_4]$ units of **2** shown by different arrowheads. For a clear illustration, arrowheads representing the dipole moments of $[\text{PbSe}_4]$ are reduced four times. (Turquoise, Ga; green, Ge; red, Se; black, Pb.)

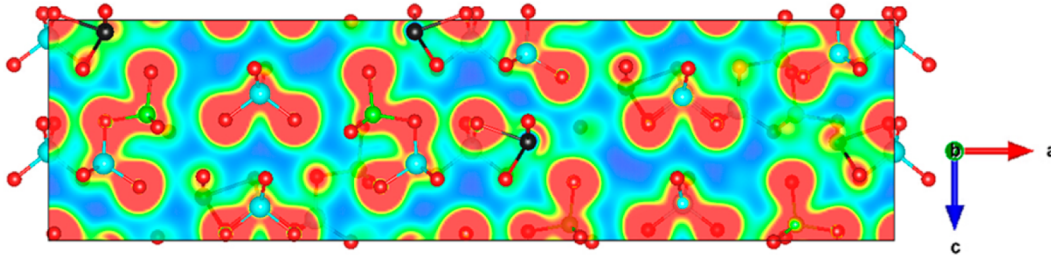


Figure 11. PED maps for compound **2** from -5 eV to the Fermi level, and the electron density is represented from blue (0.0 e/ \AA^3) to red (0.138 e/ \AA^3). The PED calculations were performed by using the VASP program.

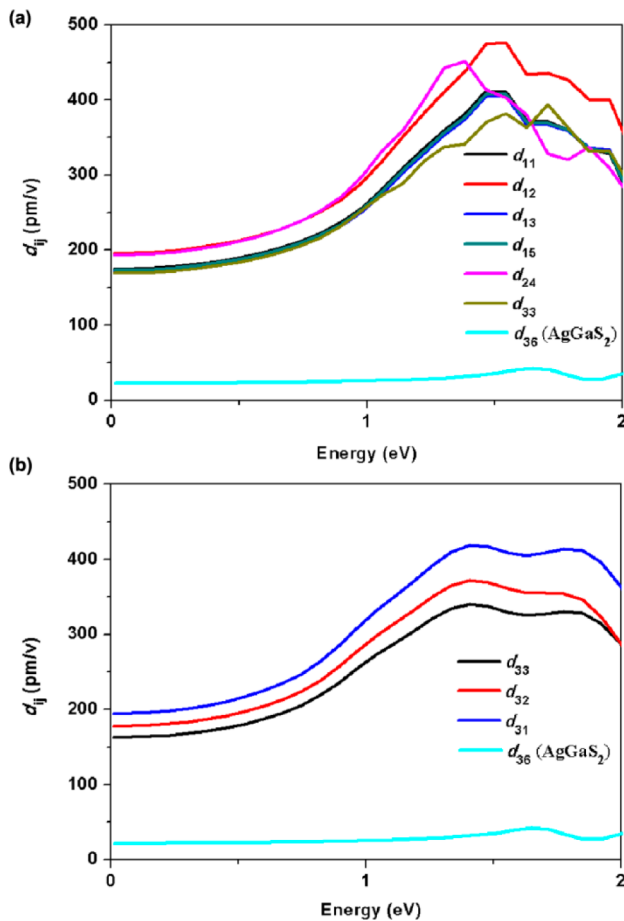


Figure 12. Calculated frequency-dependent SHG tensor components of **1** (a) and **2** (b) with d_{36} (21.2 pm/V) of AgGaS_2 as a reference.

experiments and results in the synthesis and characterization of NLO crystals in our lab show that the strategy of combining

two or more types of NCS chromophores to form an NCS crystal not only increases the probability but also improves the NLO performances of them.

■ ASSOCIATED CONTENT

● Supporting Information

The experimental and simulated X-ray diffraction patterns, X-ray crystallographic files in CIF format, TGA curves, and additional tables and figures for **1** and **2**. This material is available free of charge via the Internet at <http://pubs.acs.org>. ICSD nos. 425928 and 425929 containing the supplementary crystallographic data of this work can be obtained from the Fachinformationszentrum Karlsruhe, 76344 Eggenstein-Leopoldshafen, Germany [fax: (49) 7247-808-666; e-mail: crysdata@fiz-karlsruhe.de].

■ AUTHOR INFORMATION

Corresponding Author

*E-mail: cwd@fjirsm.ac.cn.

Notes

The authors declare no competing financial interest.

■ ACKNOWLEDGMENTS

This investigation was based on work supported by the National Basic Research Program of China (Grant 2014CB845605), the National Natural Science Foundation of China under projects 21173225, 91222004, and 21101156, and Fujian Provincial Key Laboratory of Theoretical and Computational Chemistry. We thank Prof. Ning Ye and Dr. Min Luo at FJIRSM for help with the SHG measurements and Prof. Ge Zhang and M. E. Bingxuan Li at FJIRSM for help with the LIDT's measurements.

■ REFERENCES

- (1) Nikogosyan, D. N. *Nonlinear optical crystals: A complete survey*, 1st ed.; Springer: New York, 2005.

- (2) Shunemann, C. P. *Proc. SPIE-Int. Soc. Opt. Eng.* **2007**, *6455*, 64550R–1.
- (3) Gmachl, C.; Capasso, F.; Kohler, R.; Tredicucci, A.; Hutchinson, A. L.; Sivco, D. L.; Baillargeon, J. N.; Cho, A. Y. *IEEE Circuits Devices* **2000**, *16*, 10–18.
- (4) Bera, T. K.; Jang, J. I.; Ketterson, J. B.; Kanatzidis, M. G. *J. Am. Chem. Soc.* **2009**, *131*, 75.
- (5) (a) Bordui, P. F.; Fejer, M. M. *Annu. Rev. Mater. Sci.* **1993**, *23*, 321–379. (b) Chen, C. T.; Wang, Y.; Xia, Y. N.; Wu, B. C.; Tang, D. Y.; Wu, K. C.; Zeng, W. R.; Yu, L. H.; Mei, L. F. *J. Appl. Phys.* **1995**, *77*, 2268.
- (6) (a) Jayaraman, A.; Narayananmurti, V.; Kasper, H. M.; Chin, M. A.; Maines, R. G. *Phys. Rev. B* **1976**, *14*, 3516. (b) Schunemann, P. G. *AIP Conf. Proc.* **2007**, *916*, 541–559.
- (7) Lin, X. S.; Zhang, G.; Ye, N. *Cryst. Growth Des.* **2009**, *9*, 1186–1189.
- (8) Yao, J. Y.; Mei, D. J.; Bai, L.; Lin, Z. S.; Yin, W. L.; Fu, P. Z.; Wu, Y. C. *Inorg. Chem.* **2010**, *49*, 9212–9216.
- (9) Luo, Z. Z.; Lin, C. S.; Cheng, W. D.; Zhang, H.; Zhang, W. L.; He, Z. Z. *Inorg. Chem.* **2013**, *52*, 273–279.
- (10) Luo, Z. Z.; Lin, C. S.; Zhang, W. L.; Zhang, H.; He, Z. Z.; Cheng, W. D. *Chem. Mater.* **2014**, *26*, 1093–1099.
- (11) Feng, K.; Jiang, X. X.; Kang, L.; Yin, W. L.; Hao, W. Y.; Lin, Z. S.; Yao, J. Y.; Wu, Y. C.; Chen, C. T. *Dalton Trans.* **2013**, *42*, 13635–13641.
- (12) Chung, I.; Kanatzidis, M. G. *Chem. Mater.* **2014**, *26*, 849–869.
- (13) (a) Li, F.; Hou, X. L.; Pan, S. L.; Wang, X. *Chem. Mater.* **2009**, *21*, 2846–2850. (b) Zhang, W. L.; Cheng, W. D.; Zhang, H.; Geng, L.; Lin, C. S.; He, Z. Z. *J. Am. Chem. Soc.* **2010**, *132*, 1508–1509. (c) Nguyen, S. D.; Yeon, J.; Kim, S. H.; Halasyamani, P. S. *J. Am. Chem. Soc.* **2011**, *133*, 12422–12425.
- (14) Luo, Z. Z.; Lin, C. S.; Cui, H. H.; Zhang, W. L.; Zhang, H.; He, Z. Z.; Cheng, W. D. *Chem. Mater.* **2014**, *26*, 2743–2749.
- (15) CrystalClear, version 1.3.5; Rigaku Corp.: The Woodlands, TX, 1999.
- (16) Sheldrick, G. M. *SHELXL-97: Program for Crystal Structure Solution*; University of Göttingen: Göttingen, Germany, 1997.
- (17) Spek, A. L. *J. Appl. Crystallogr.* **2003**, *36*, 7.
- (18) Petricek, V.; Dusek, M.; Palatinus, L. Z. *Kristallogr.* **2014**, *299* (5), 345–352.
- (19) Kortüm, G. *Reflectance Spectroscopy*; Springer -Verlag: New York, 1969.
- (20) Hervieu, M.; Perez, G.; Hagenmuller, P. *Bull. Soc. Chim. France* **1967**, *6*, 2189–2194.
- (21) Zhang, M. J.; Jiang, X. M.; Zhou, L. J.; Guo, G. C. *J. Mater. Chem. C* **2013**, *1*, 4754–4760.
- (22) Clark, S. J.; Segall, M. D.; Pickard, C. J.; Hasnip, P. J.; Probert, M. J.; Refson, K.; Payne, M. C. Z. *Kristallogr.* **2005**, *220*, 567–570.
- (23) Perdew, J. P.; Burke, K.; Ernzerhof, M. *Phys. Rev. Lett.* **1996**, *77*, 3865.
- (24) Dudarev, S. L.; Botton, G. A.; Savrasov, S. Y. C.; Humphreys, J.; Sutton, A. P. *Phys. Rev. B* **1998**, *57*, 1505.
- (25) Kresse, G.; Furthmüller, J. *Comput. Mater. Sci.* **1996**, *6*, 15.
- (26) Boyd, R. W. *Nonlinear Optics*; Academic Press, New York, 1992, 21–47.
- (27) Poudeu, P. F. P.; Takas, N.; Anglin, C.; Eastwood, J.; Rivera, A. *J. Am. Chem. Soc.* **2010**, *132*, 5751–5760.
- (28) Pocha, R.; Johrendt, D.; Ni, B.; Abd-Elmeguid, M. M. *J. Am. Chem. Soc.* **2005**, *127*, 8732–8740.
- (29) Vaju, C.; Cario, L.; Corraze, B.; Janod, E.; Dubost, V.; Cren, T.; Roditchev, D.; Braithwaite, D.; Chauvet, O. *Adv. Mater.* **2008**, *20*, 2760–2765.
- (30) Yin, W. L.; Feng, K.; He, R.; Mei, D. J.; Lin, Z. H.; Yao, J. Y.; Wu, Y. C. *Dalton Trans.* **2012**, *41*, 5653–5661.
- (31) Woolley, J. C.; Goodchild, R. G.; Hughes, O. H.; Lopez-Rivera, S. A.; Pamplin, B. R. *Jpn. J. Appl. Phys.* **1980**, *19*, 145–148.
- (32) Geng, L.; Cheng, W. D.; Lin, C. S.; Zhang, W. L.; Zhang, H.; He, Z. Z. *Inorg. Chem.* **2011**, *50*, 5679–5686.
- (33) Eisenmann, B.; Hofmann, A. Z. *Anorg. Allg. Chem.* **1990**, *580*, 151–159.
- (34) Eisenmann, B.; Jakowski, M.; Schaefer, H. Z. *Naturforsch., Teil B: Anorg. Chem.* **1983**, *38*, 1581–1584.
- (35) Liu, J. W.; Wang, P.; Chen, L. *Inorg. Chem.* **2011**, *50*, 5706–5713.
- (36) Chen, M. C.; Li, L. H.; Chen, Y. B.; Chen, L. *J. Am. Chem. Soc.* **2011**, *133*, 4617–4624.
- (37) Zhao, H. J.; Zhang, Y. F.; Chen, L. *J. Am. Chem. Soc.* **2012**, *134*, 1993–1995.
- (38) Wu, K. C.; Chen, C. T. *Appl. Phys. A: Mater. Sci. Process.* **1992**, *54*, 209–220.
- (39) (a) Dmitriev, V. G.; Gurzadyan, G. G.; Nikogosyan, D. N. *Handbook of Nonlinear Optical Crystals*; Springer: New York, 1999. (b) Ebrahim-Zadeh, M.; Sorokina, I. T. *Mid-Infrared Coherent Sources and Applications*; NATO Science for Peace and Security Series B: Physics and Biophysics; Springer: New York, 2007.
- (40) Hopkins, F. K. *Opt. Photonics News* **1998**, *9*, 32–38.
- (41) Perdew, J. P.; Levy, M. *Phys. Rev. Lett.* **1983**, *51*, 1884–1887.
- (42) Perdew, J. P.; Chevary, J. A.; Vosko, S. H.; Jackson, K. A.; Pederson, M. R.; Singh, D. J.; Fiolhais, C. *Phys. Rev. B* **1992**, *46*, 6671–6687.
- (43) Chen, M. C.; Li, P.; Zhou, L. J.; Li, L. H.; Chen, L. *Inorg. Chem.* **2011**, *50*, 12402–12404.
- (44) Mei, D. J.; Gong, P. F.; Lin, Z. S.; Feng, K.; Yao, J. Y.; Huan, F. Q.; Wu, Y. C. *CrystEngComm* **2014**, *16*, 6836–6840.